A Transfer Learning Approach for UAV Path Design with Connectivity Outage Constraint

Gianluca Fontanesi, *Graduate Student Member, IEEE*, Anding Zhu, *Fellow, IEEE*, Mahnaz Arvaneh, *Member, IEEE*, and Hamed Ahmadi, *Senior Member, IEEE*

Abstract—The connectivity-aware path design is crucial in the effective deployment of autonomous Unmanned Aerial Vehicles (UAVs). Recently, Reinforcement Learning (RL) algorithms have become the popular approach to solving this type of complex problem, but RL algorithms suffer slow convergence. In this paper, we propose a Transfer Learning (TL) approach, where we use a teacher policy previously trained in an old domain to boost the path learning of the agent in the new domain. As the exploration processes and the training continue, the agent refines the path design in the new domain based on the subsequent interactions with the environment. We evaluate our approach considering an old domain at sub-6 GHz and a new domain at millimeter Wave (mmWave). The teacher path policy, previously trained at sub-6 GHz path, is the solution to a connectivity-aware path problem that we formulate as a constrained Markov Decision Process (CMDP). We employ a Lyapunov-based model-free Deep Q-Network (DQN) to solve the path design at sub-6 GHz that guarantees connectivity constraint satisfaction. We empirically demonstrate the effectiveness of our approach for different urban environment scenarios. The results demonstrate that our proposed approach is capable of reducing the training time considerably at mmWave.

Index Terms—Cellular networks, deep reinforcement learning, path design, transfer learning, Unmanned Aerial Vehicle (UAV).

I. INTRODUCTION

Unmanned Aerial Vehicles (UAVs) are expected to be a promising solution in diverse applications, such as fast delivery, surveillance and disaster management thanks to their easy deployment and high mobility [1]. From the standpoint of wireless communications, on one hand, ground Base Stations (BSs) can be leveraged to support UAVs as flying User Equipments (UEs) for remote operations and high data rate transmissions [2]. On the other hand, cellular networks can be used to provide a Backhaul (BH), or Fronthaul (FH) link to UAVs when deployed as wireless BSs or Remote Radio Heads (RRHs). UAV-BSs/RRHs offer rapid deployment of on-demand communication in hotspots and provide emergency service operations [3], [4].

G. Fontanesi and A. Zhu are with the School of Electrical and Electronic Engineering, University College Dublin, Dublin 4, D04 V1W8, Ireland (e-mail: gianluca.fontanesi@ucdconnect.ie; anding.zhu@ucd.ie).

H. Ahmadi is with the Department of Electronic Engineering, University of York, Heslington, York YO10 5DD, United Kingdom, and with the School of Electrical and Electronic Engineering, University College Dublin, Dublin 4, D04 V1W8, Ireland (e-mail: hamed.ahmadi@ucd.ie).

M. Arvaneh is with the Automatic Control and Systems Engineering, University of Sheffield, UK(e-mail: m.arvaneh@sheffield.ac.uk)

A high quality and reliable ground to air link along the entire path [5] represents a crucial challenge for the effective deployment of UAVs in the above scenarios. An efficient UAV path design shall thus optimize the UAV path to minimize the travelling time and comply with the quality-of-connectivity constraint on the ground to air link. However, designing a connectivity-aware path is particularly challenging for two main reasons. First, conventional cellular networks are equipped with downtilted antennas to serve UEs on the ground. Consequently, the ground to air link is likely capacity limited or prone to low connectivity at specific areas or heights [6]. Second, when UAVs are deployed in unseen environments, the unavailability of knowledge about the environment increases the complexity of the path design.

A. State of the art

Prior solutions to the UAV path optimization problem usually use conventional optimization techniques. Works in [7], [8], [9], [10] discuss graph-search methods, whereas a dynamic programming approach is used in [11]. These approaches reformulate the corresponding non-convex path planning optimization problems in a more tractable form that suffers from poor scalability and is based on simplified assumptions on the antenna and propagation models.

The above issues can be circumvented by exploiting detailed information on the propagation channels in a given geographical area, such as radio maps. The work in [12] utilizes a radio map of the environment to find the shortest path using graph algorithms. The radio map is assumed known as a priori. In [13], the authors first reconstruct the radio map of the area to estimate the channel parameters. Then, the path is optimized to maximize the data collected from the ground. Similarly, in [10], [14], [15], the UAV uses a coverage map that provides accurate locations of coverage holes in the network to maintain effective communication with the ground during the flight while moving from a starting to a final position in the shortest amount of time. A^* is thus applied for finding the shortest (or approximately shortest) path in a much shorter computation time than canonical Dijkstra's algorithm, by considering a smaller search subspace.

The above works show that the availability of radio or coverage maps makes algorithms like A^* attractive for UAV path design problems. However, the assumption of full map availability is generally impractical since radio and coverage maps need to be estimated by collecting beforehand many radio measurements in a specific environment [16]. Notably,

using a A^* algorithm for UAV path design would require the availability of coverage maps for each UAV potential and allowed height in the area where the UAV is planned to fly. This is hard and expensive to be reached in practice.

In Reinforcement Learning (RL) algorithms, such as the one proposed in this paper, prior knowledge of the environment like radio and coverage maps is not required. RL algorithms can learn the environment and autonomously determine the optimal path through UAV-environment interactions and only with UAV's measured data, such as the received signal power. For this reason, applying RL algorithms in the UAV path design has received increasing interest. In [17], a Q-learning path algorithm is proposed to design UAV path. A UAV interacts with the environment collecting positive or negative feedback. The algorithm considers the continuous and total outage during the UAV path to prevent the UAV from losing communication with the ground. However, when the size of the considered flying environment increases, Q-Table becomes too large and tabular methods such as Q-learning don't represent an efficient solution. It is thus beneficial for UAV path planning to use Deep Reinforcement Learning (DRL) methods that combine RL with Deep Neural Network (DNN) to address more challenging tasks. In [18], the authors study the use of Deep Q-Network (DQN) to minimize the weighted sum of the UAV mission completion time and the communication outage duration. In [19], the connectivity aware path is proposed in a similar DQN fashion, but it also includes the optimal selection of the ground BS transmitter.

One major issue of a model-free approach in UAV communication, such as DQN, is the need for a relatively high number of learning trials to converge. During the initial training, the algorithm performance is poor and improves only when enough information about the scenario environment is collected. However, this lengthy training is equivalent to thousands of flights where the reliability of the ground to air link is not guaranteed and it is costly, due to the UAV's onboard battery and energy waste. Preliminary works have investigated methods to improve the learning efficiency. Using a model-based RL, the work in [18] uses the measurements collected during the flights in the training to build a radio map of the environment. The radio map is exploited to generate simulated UAV trajectories and predict their corresponding outage duration. In [20], the radio map of the environment is built in a distributed fashion using Federated Learning (FL) through the collaboration of multiple UAVs. The joint flight and connectivity optimization problem is then solved collectively. The work in [19] reuses past successful trajectories to imitate the same behavior and achieve faster convergence.

B. Contribution

The above mentioned solutions contribute to reducing the algorithms' execution time but still fail to generalize when applied to different unseen scenarios. In fact, these approaches are tailored for a single environment only or used to build a radio map of the environment [17-18]. This affects the ability of the UAV to make good decisions when facing an unseen environment. As a consequence, the agent would require to re-run the lengthy training process for any new environment faced by the UAV.

For these reasons, we believe that, to make DRL based solutions attractive for UAV connectivity aware path design in real scenarios, there is a need for a framework that can significantly improve the performance in unseen environments. Motivated by this challenge, we address the UAV connectivity aware path using a Transfer Learning (TL) approach. TL is the process of utilizing knowledge gained from other tasks, or prior knowledge, to benefit the target task's learning process. The core idea of our paper is to transfer the experience gained in learning to perform the proposed robust-DDQN path design in a old domain to help improving learning performance of the proposed DDQN path design in a new domain. Our method for transfer learning translates advice, or preferences, from a teacher path policy learned in an old domain D_1 at f_1 into a new domain D_2 at f_2. Since future wireless networks will support the sub-6 GHz and mmWave frequency ranges [21], we believe that a different frequency band represents an interesting and practical use case of unseen environment in UAV path design. Our approach hinges on a Lyapunov method in the search for a robust teacher policy that can effectively guarantee the connectivity constraint satisfaction during training. To test our TL approach in a challenging scenario, we consider sub-6 GHz and millimeter Wave (mmWave) frequency bands, which have different propagation characteristics (blockage sensitivity and scattering loss) and bandwidth availability. While other papers focused on exploiting the correlation between these two frequencies [22], we exploit that TL approaches are suitable for equivalent or different domains [23]. To demonstrate the generality of our approach we have considered different blockage scenarios corresponding to the Urban, Dense Urban and High Rise environments.

To better highlight the contribution of this paper, Table I presents a comparison of this work with different works in the literature. A systematic search was implemented to identify the most important related works in the connectivity aware design. The research is restricted to journal and conference papers only and keywords such as UAV, connectivity and disconnectivity constraint, path and prior knowledge. It can be noted that the connectivity outage constraint is formulated in different forms to cater for different UAV application scenarios flexibly. We propose a framework that can solve the communication-aware trajectory problem efficiently without the assumptions of coverage maps while, at the same time, representing a robust teacher policy to improve the training in new environments through TL. To the authors' best knowledge, while TL is becoming a crucial topic in DRL and various domains [24], [25], this is one of the first times Teacher Advice TL is combined with a Lyapunov approach and applied to the UAV connectivity aware path design. The TL method allows us to create and incorporate prior knowledge in our DRL solution without performing expensive measurement campaigns, speed up the learning process, and optimally solve the optimization problem.

The contribution of this paper can be listed as follows:
- First, we formulate a 3-D UAV path problem under ground to air link connectivity outage constraint as Con-

TABLE I: Comparisons between Related Studies on UAV path Optimization with Connectivity Constraint, where SNR is Signal to Noise Ratio, PER stands for Priority Experience Replay, and TD is Temporal Difference.

Ref.	Connectivity Constraint	UAV Role	Prior Knowledge	Technique
[7]	Minimum Target SNR	UAV-UE	✗	Dijkstra Algorithm
[8]	Backhaul Constraint - no Minimum Rate	UAV-BS	✗	Dijkstra Algorithm
[9]	Maximum Outage Duration	UAV-UE	✗	Graph Theory, Convex Optim.
[10]	Minimum Throughput	UAV-UE	Throughput Map	A^* Algorithm
[11]	Maximum Continuous Disconnectivity Time	UAV-UE	✗	Dynamic Programming
[12]	Minimum Target SNR	UAV-UE	Radio Map	Dijkstra Algorithm
[13]	Minimum Target SNR	UAV-UE	Radio Map	Dynamic Programming
[14]	Connectivity Outage Ratio and Duration	UAV-UE	Coverage Maps	Graph Search Method
[15]	Minimum Target SNR	UAV-UE	Coverage Map	A^* Algorithm
[16]	Minimum Target SNR	UAV-UE	Radio Map	Graph Search Method
[17]	Maximum Continuous and Total Disconnectivity Time	UAV-UE	✗	Double Q-Learning
[18]	Total Disconnectivity Time	UAV-UE	✗	Model-based DQN (Dyna)
[19]	Maximum Continuous Disconnectivity Time	UAV-UE	Radio Map	DRL
[20]	Maximum Continuous Connectivity Outage	UAV-UE	Radio Map	Federated Learning
[24]	✗	UAV-BS	Environ. Model	DDQN, TL
[26]	Minimum Target SNR at UE	UAV-BS	Coverage Bitmap	PER DRL
[27]	Disconnection Duration	UAV-UE	✗	TD Learning
[28]	Connectivity Outage Ratio	UAV-UE	✗	Dijkstra with Intersection
[29]	Total Connectivity Outage Time	UAV-UE	✗	Dijkstra with Intersection
[30]	UAV Disconnection Duration	UAV-UE	✗	Decentralized DRL
[31]	UAV Disconnection Duration	UAV-UE	✗	DRL
[32]	Minimum Target SNR at UE	UAV-BS	✗	Q-Learning
[33]	Backhaul Constraint - Minimum Rate	UAV-BS	Channel Gain	Interior Method
[34]	Disconnectivity Rate	UAV-cargo	Connectivity Heatmap	Dynamic Programming
[35]	Total Radio Failures	UAV-UE	✗	DDQN
This Work	Outage on Ground to Air Link	UAV-UE, UAV-BS	Teacher Policy	Lyapunov robust-DDQN

strained Markov Decision Process (CMDP).

- Thus, we propose a Lyapunov approach to solve the CMDP and obtain a strategy that ensures the UAV reaches the destination while respecting the connectivity outage constraint at all times. We then develop a robust-Double Deep Q-Network (DDQN) based algorithm to learn an optimal policy at f_1.
- Utilizing the concepts of teacher advice and TL, we present a novel algorithm that uses the derived trained policy as a teacher policy at sub-6 GHz to guide the exploration process at mmWave and reduce the training time.
- We first demonstrate the efficiency of the robust-DDQN comparing its performance to a benchmark conventional Dueling DDQN. At sub-6 GHz frequency band, we show that our approach can better explore the environment and achieve higher mission success.
- Finally, we also evaluate the proposed teacher advice and TL strategy in terms of the percentage of successful missions. Results show that using a teacher policy trained at sub-6 GHz frequency band significantly speeds up the learning process at mmWave than starting the training from scratch. Moreover, the robust-DDQN results in a better teacher policy than the state of the art Dueling DDQN.

The system model and the problem formulation are presented in Section II. In Section III, we transform the problem into a CMDP and propose a robust-DDQN-based trajecotry design algorithm to play as teacher for TL. The TL approach is presented in Section IV while the Numerical Results are in Section V. Finally, Section VI concludes the paper.

II. SYSTEM MODEL AND PROBLEM FORMULATION

We consider a set, $\mathcal{G}$, of B cellular BSs providing downlink wireless service in a geographical area of interest $X \in \mathbb{R}^3$. UAVs can be deployed to reach an area of interest, $F \in X$, as UAVs-UE for delivery of supplies, or UAVs as BS or RRH to provide service to a demand hotspot [8]. We assume that the path of the UAV starts from a random starting position $\mathbf{q}_I = [x_0, y_0, h_0] \in X, \notin F$, and ends in a final predetermined position $\mathbf{q}_F = [x_F, y_F, h_F]^T \in F$ for a duration T. For the convenience of illustration, we divide the finite UAV mission completion time T into a sequence of discrete time instances $t_1, t_2, ... t_\omega$ such that $T = \omega \Delta_T$ and $|t_n - t_{n-1}| \leq \Delta_T$. The UAV path can be thus approximated by the sequence $\{q_n\}_{n=1}^{\omega}$ where each step point at instant n is thus described by its discrete coordinates $\mathbf{q_n} = [x_n, y_n, h_n]$. The location and the transmit power P_{BS} of the ground BSs can be assumed as known. We also assume that all ground BSs have equal altitude h_{BS}. Each BS and the UAV can operate at f_1 and f_2 but we assume that data transmission occurs in a single frequency band at a time.

Let $\mathbf{b_m} = [x_m, y_m, h_{BS}]$ the coordinate of the m-th ground BS in a three-dimensional coordinate system, the distance between the UAV and the m-th ground BS at step n is given by:

$$d_{m,n} = \|\mathbf{q_n} - \mathbf{b_m}\|, \quad m \in \mathcal{G}. \tag{1}$$

Next, we describe the channel model and formulate the problem.

A. Ground-to-Air Channel Model

We consider wireless ground-to-air channel ground BS-UAV characterized by deterministic large scale path loss and random small-scale fading. We consider a generic urban environment where the ground BS-UAV link might be occasionally blocked

TABLE II: List of Notations and Symbols Summary

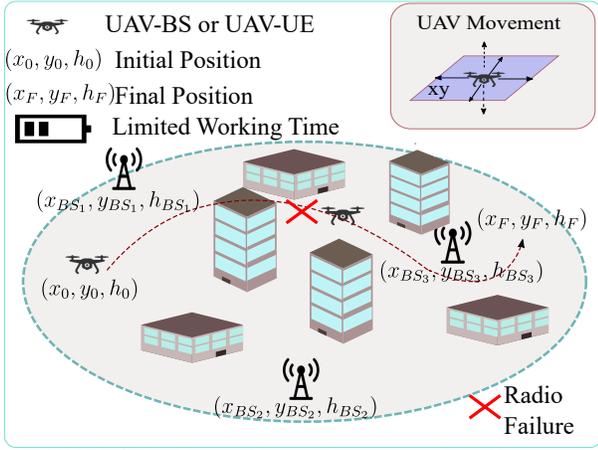| Notation	Description	Notation	Description
X	Area of Interest	Π	Set of markov stationary policies
$\mathcal{G}$	The set of GBSs	$\mathcal{C}_\pi()$	Expected cumulative cost function
$V_{\max}$	Maximum UAV speed	$\mathcal{D}_\pi()$	Expected cumulative constraint function
N	Path duration	π_B	Baseline policy
$\overline{N}$	Maximum UAV mission duration	L	Lyapunov function
$\mathbf{q}_I$	Path starting location	$T_{\pi,h}$	Bellman operator
$\mathbf{q}_F$	Path final location	$\epsilon, \hat{\epsilon}$	Auxiliary constraint
q_n	UAV Discrete path step n	F_L	Set of robust policies
$\mathbf{b_m}$	m-th Ground BS coordinate	L_ϵ	Approximated Lyapunov function
h_{BS}	BS height	$Q_D(s,a,\theta)$	Constraint value network
$d_{m,n}$	Distance between the m_{th} GBS and the UAV	$Q_L(q_n,a)$	Lyapunov value function
$L()$	Path loss model	$Q_C(s,a,\theta)$	Cost value network
α_L, α_{NL}	Path loss exponents for LoS and NLoS	$Q_T(q_n,a)$	Stopping time value network
X_L, X_{NL}	LoS, NLoS intercepts	p_c, p_d	Samples priority
ϕ_1, ϕ_2	Antenna tilt at f_1, f_2	δ	TD-error
P_{TX}	Transmit power of ground BS	π_T	Teacher policy
σ_n^2	Thermal noise power	H	Prioritized replay memory
h, m_v	Fading, Nakagami fading parameter	B	Minibatch
$\gamma_{m,n}, \bar{\gamma}$	SINR, SINR threshold	Σ, Υ	Known, Unknown space
S_O	Subset of outage Regions	D_1, D_2	Old domain, new domain
$F(\mathbf{q}_n)$	Radio failure indicator	C, Z	Size of known space memory, size
d_O	Connectivity outage constraint	Θ, Λ	Density threshold, Risk function
d_{th}	Max tolerated radio failures	π_2	Policy in new domain

Fig. 1: UAV is flying in an urban environment where the ground BS-UAV link might be occasionally blocked by buildings based on the building distribution and UAV height, leading to radio failures.

by obstacles and buildings based on the building distribution in X and UAV height. In order to present the results more generically, the path loss at f_1 and f_2 between the mth ground BS and the UAV can be modeled to take into account the Line of Sight (LoS) and Non-Line of Sight (NLoS) case as for [5]:

$$L(d) = \begin{cases} X_L d_{m,n}^{-\alpha_L}; \\ X_{NL} d_{m,n}^{-\alpha_{NL}}; \end{cases} \quad (2)$$

where $d_{m,n}$ is the ground BS-UAV distance as for (1), and parameters α_L, α_{NL} and X_L, X_{NL} represent, respectively, the path loss exponent for LoS/NLoS and the path loss at 1 meter distance. To capture the LoS and NLoS effect at sub-6 GHz, we model the small scale fading power as Rician for the LoS and as Rayleigh for the NLoS link [18]. At mmWave, we model the small scale fading power $h_{0,i}^2$ with i {$LoS, NLoS$} as a Nakagami-m_v fading model [5]. Accordingly, the fading power at mmWave follows a Gamma distribution with $\mathbb{E}[h_0^2] = 1$.

1) Antenna Model: We adopt the three-sectors antenna model as characterized by 3rd Generation Partnership Project (3GPP) specification [36]. Similar to [37], we consider that each sector is separated by $120°$ and equipped with a vertical N-element Uniform Linear Array (ULA) tilted with angle ϕ_1 at f_1 and a Uniform Planar Square Array (UPA) $N \times N$ tilted with angle ϕ_2 at f_2. The dB gain experienced by a ray with elevation and azimuth angle pair θ, ϕ due to the effect of the element radiation pattern can be expressed as:

$$A_E^{3GPP}(\theta,\phi) = G_{max} - \min\{-[A_{E,V}(\theta) + A_{E,H}(\phi)], A_m\} \quad (3)$$

where $G_{max} = 8$ dBi is the maximum directional gain of the antenna element. The 3GPP element radiation pattern of each single antenna element is composed of horizontal and vertical radiation patterns $A_{E,H}(\phi)$ $A_{E,V}(\theta)$. Specifically, this last pattern $A_{E,V}(\theta)$ is obtained as

$$A_{E,V}(\theta) = -\min\left\{ 12\left(\frac{\theta - 90°}{\theta_{3dB}}\right)^2, SLA_V \right\} \quad (4)$$

where $\theta_{3dB} = 65°$ is the vertical beamwidth, and $SLA_V = 30$ dB is the side-lobe level limit. Similarly, the horizontal pattern is computed as

$$A_{E,H}(\phi) = -\min\left\{ 12\left(\frac{\phi}{\phi_{3dB}}\right)^2, A_m \right\} \quad (5)$$

where $\phi_{3dB} = 65°$ and $A_m = 30$ dB is the front-back ratio. The relationship between the array radiation pattern and a single pattern is defined as $A_A(\theta,\phi,n) = A_E(\theta,\phi) + AF(\theta,\phi,n)$, where n is the number of antenna elements and $AF(\theta,\phi,n)$ is the array factor. $AF(\theta,\phi,n)$ is given in [37] as:

$$AF(\theta,\phi,n) = 10\log_{10}\left[1 + \rho\left(|\mathbf{a} \cdot \mathbf{w}^T|\right)\right] \quad (6)$$

where ρ represents the correlation coefficient set to unity, $\mathbf{a}$ is the amplitude vector and $\mathbf{w}$ is the beamforming vector. The definition of $\mathbf{w}$ can be found in [19], [37] and is omitted here.

As in [19], [37], we consider an equal and fixed amplitude for the antenna elements. As a consequence, $\mathbf{a}$ is set to $(\frac{1}{\sqrt{n}})$ and we leave the integration of optimized weights in beamforming techniques for future investigation.

Finally, we assume the UAV is equipped with a conventional isotropic antenna of unitary gain in any direction to mantain low complexity and cost.

For simplicity, but without loss of generality, we focus on one typical UAV. At any time step during the UAV's mission, the UAV associates with one ground BS's sector only, following a maximum Signal-to-Noise-plus-Interference Ratio (SINR) scheme [5]. The maximum instantaneous SINR received at the omnidirectional UAV from the attached m-th ground BS can be defined as:

$$\gamma_{m,n} = \frac{P_{BS}L(d_{m,n})h_0^2(d_{m,n})g_{m^*,j^*}}{\sigma^2 + I_t}, \tag{7}$$

where $L()$ is the path loss, the random variable h accounts for the fading, and I_t the interference associated with the non-attached BSs. The term

$$g_{m^*,j^*} = \underset{m \in \mathcal{G}, j \in \mathcal{J}}{\arg\max} \, g_{m,j}$$

is the antenna gain from the j-th sector of the m-th ground BS and $j \in \mathcal{J} = \{1, 2, 3\}$ denotes the set of sectors.

For a given SINR threshold $\bar{\gamma}$, an outage occurs at step n if at the UAV the condition $\gamma_{m,n} \leq \bar{\gamma}$ is not satisfied. The resulting outage probability can be denoted as

$$P_{outage}(\mathbf{q}_n, m) = Pr(\gamma_{m,n} < \bar{\gamma}), \tag{8}$$

where Pr is the probability of the event taken with respect of the randomness of the fading. Note that the value of Δ_T can be considered small enough to satisfy $\Delta_T V << h_n$, and in the generic flying step n, the UAV can be considered stationary [18], [38]. Let us define a radio failure indicator on the ground to air link as

$$F(\mathbf{q}_n) = \begin{cases} 1, & \text{if } P_{outage}(\mathbf{q}_n, m) \geq \bar{P}_{th} \\ 0, & \text{otherwise.} \end{cases} \tag{9}$$

Thus, we can introduce S_O as the subset of outage regions where (9) holds true. Then, for an arbitrary outage probability threshold $\bar{P}_{th}$ and a given path q_n with $\mathbf{q}_I \notin S_O$, the connectivity outage constraint d_O can be expressed as

$$d_O = \sum_{n=1}^{N} F(\mathbf{q}_n). \tag{10}$$

B. Problem Formulation

We would like the UAV to reach the destination in the shortest possible number of moves, while keeping the outage events lower than d_{th}. The UAV's velocity is limited to its maximum speed. We consider that during its mission, the UAV moves at constant $V = V_{\max}$. This assumption of constant maximum speed makes the mathematical modeling more tractable as the variable speed will have control and/or aerodynamic related reasons which are out of our control and scope of work. In addition, using UAV's maximum speed allows the UAV to reach the destination in the minimum path

steps. The UAV maximum speed used in this paper to derive the numerical results is a realistic and aerodynamic supported maximum speed, used in several related connectivity-aware path design works [28], [18], [20]. Thus, the mission variable T can be expressed as $T = \frac{\sum_{n=1}^{\omega} \|\mathbf{q}_n - \mathbf{q}_{n-1}\|}{V_{Max}}$ and optimization problem can be formulated as in (11).

$$\min_{\omega} \quad \sum_{n=1}^{\omega} \|\mathbf{q}_n - \mathbf{q_{n-1}}\| \tag{11a}$$

$$\text{s.t.} \quad \mathbf{q}_0 = \mathbf{q}_I, \mathbf{q}_N = \mathbf{q}_F \tag{11b}$$

$$h_n > h_{BS} \tag{11c}$$

$$\|\mathbf{q}_n - \mathbf{q}_{n-1}\| \leq \Delta_T V_{\max}, \tag{11d}$$

$$d_O \leq d_{th}, \tag{11e}$$

$$\omega \leq \bar{N}. \tag{11f}$$

Variable ω represents the mission completion steps. The constraint (11b) guarantees the initial and final points, (11c) prevents the collision between the UAV and the ground BSs. (11d) constraints on the UAV's maximum speed. The connectivity constraint d_O must not exceed a predefined threshold d_{th}. For this reason, (11e) defines the connectivity outage duration tolerance. Constant $\bar{N}$ in (11f) is the upper bound on the UAV steps to take into account the limited UAV endurance. In our design, d_{th} is not fixed but can be tuned to suit different application scenarios. Longer paths may help the UAV avoid S_O areas and satisfy stringent values of d_{th}. In scenarios where the UAV is deployed for timing intervention a higher d_{th} might be tolerated to achieve shorter paths. Although UAV-UE and UAV-BS cases generally have different design problems, the above connectivity constraint path optimization applies to both the scenarios from the ground to air link point of view.

The connectivity-aware problem (11) is a non-convex optimization problem that is generally intractable to solve via conventional optimization techniques. The Proof of NP-hardness of a similar path design problem can be found in [28] and omitted here. In addition, a closed-form expression of the outage probability (8) used to compute (11e) is highly dependent on the network topology, channel fading and antenna gain. In our previous work [5], taking into account the channel characteristics at f_1 and f_2, we have investigated a stochastic geometry approach to deduce a tractable form of P_{outage}. However, statistical approaches provide useful insights on the average performance of the network but they don't capture the actual complexity of the local environment where the UAVs are deployed.

RL approaches, that interact iteratively with the environment, circumvent these issues solving the path optimization problem using the power measurements at the UAV in a certain time step. While RL algorithms for the design of UAV connectivity aware path have been proposed already in literature (Table I), this paper aims to propose a novel TL approach to improve the efficiency of DQN for UAV path design. More specifically, adopting the dual band system model described in Section II, we focus on two fundamental problems: (i) how can a robust policy derived at f_1 be used to infer the path at f_2, (ii) what is the best algorithm solution of (11) at f_1 to act as teacher for f_2, solving (i).

Next, to determine a set of suitable policies to the connectivity aware problem, we propose a Lyapunov approach method to the UAV path design. Finally, based on the Lyapunov approach, we develop a teacher robust-DDQN algorithm.

III. CREATION OF A ROBUST TEACHER POLICY

The position of UAV at step q_{n+1} depends on the position and moving direction chosen by the agent at step q_n. Hence, the UAV's flight process can be regarded as a discrete-time CMDP, an extension of the Markov Decision Process (MDP) framework that suits optimization problems as (11), where agents optimize one objective while satisfying cost constraints. Note that we assume the UAV to be controlled by a dedicated agent and the terms agent and UAV will be used hereafter interchangeably.

A. Problem Formulation as CMDP

Each CMDP consists of a 7-tuple $\langle \mathcal{S}, \mathcal{A}, \mathcal{P}, c, d, \alpha, d_{th} \rangle$. In this work $\mathcal{S}$ is the space state consisting of the UAV positions within the feasible flying region with single state q_n. The agent's action corresponds to one of the UAV's flying directions, that together represent the action space $\mathcal{A}$. The UAV moves in a custom environment consisting of area X covered by the dual band network. The immediate cost function is modeled as $c(q_n, a_n) = -1 - \|q_n - q_F\|$. The first term penalizes the UAV for each move and accounts for UAV battery usage. At the same time, the second cost term measures the relative distance to the destination and encourages the UAV to complete its mission in the shortest possible number of moves. We define the immediate constraint cost $d(q_n)$ as the radio failure indicator $F(q_n)$ in (9), d_{th} is an upper bound on the expected cumulative constraint cost. Lastly, variable $\alpha \in [0, 1]$ in $\langle \mathcal{S}, \mathcal{A}, \mathcal{P}, c, d, \alpha, d_{th} \rangle$ represents the discount factor.

Under this framework, at any step n, the UAV moves from q_n to q_{n+1} during step length Δ_T at speed V_{max} based on the action a_n, selected according the current policy π. We define a policy $\pi(a | q_n)$ as the condition probability to take action a given the state q_n. After taking action a_n, the UAV interacts with the environment receiving the immediate cost $c(q_n, a_n)$ and constraint cost $d(q_n)$. A sequence of interactions leads to a terminal or goal state, where an episode ends. For the computation $F(q_n)$, note that Δ_T usually contains many channel coherence blocks due to small-scale fading. As a result, it can be assumed that as long as the UAV performs signal measurements sufficiently frequently, the outage probability (8) can be evaluated by its empirical value $\hat{P}_{outage}(q_n, m) = 1/J \sum_{j=1}^{J} O(q_n, m)$ where $J \gg 1$ and $O()$ is 1 if $\gamma_{m,n} \leq \bar{\gamma}$ and 0 otherwise [18].

To complete the CMDP formulation of (11) we need to formalize the constraint (11e) that bounds the total frequency of visiting S_O with a predefined threshold d_{th} into a CMDP. We rewrite (11e) using the immediate constraint notation $d(q_n) = \mathbf{1}\{q_n \in S_O\}$, where $\mathbf{1}\{x\}$ denotes the indicator function so that its value is 1 if $x \in S_O$ and 0 otherwise [39]. Thus constraint (11e) becomes

$$\mathbb{E}[\sum_{n=1}^{N} \mathbf{1}\{q_n \in S_O\} \mid q_I, \pi] \leq d_{th}. \tag{12}$$

Let us now denote Π the set of Markov stationary policies with policy element π, such that $\Pi(q_n) = \{\pi(\cdot | q_n) : \mathcal{S} \to \mathcal{R}_{\geq 0s} : \sum_a \pi(a | q_n) = 1\}, \forall q_n \in \mathcal{S}$ follows from the stationary property. Given a policy $\pi \in \Pi$ that maps states to actions and an initial state q_I, we can define the expected cumulative cost function as

$$\mathcal{C}_\pi(q_I) = \mathbb{E}\left[\sum_{n=1}^{N} c(q_n, a_n) \mid q_I, \pi \right], \tag{13}$$

and the robustness constraint function as

$$\mathcal{D}_\pi(q_I) = \mathbb{E}\left[\sum_{n=1}^{N} d(q_n) \mid q_I, \pi \right]. \tag{14}$$

The optimization problem (11) becomes then

$$\pi^* \in \min_\pi \mathbb{E}\left[\sum_{n=1}^{N} c(q_n, a_n) \mid q_I, \pi \right] \tag{15a}$$

$$\text{s.t. } \mathbb{E}\left[\sum_{n=1}^{N} d(q_n) \mid q_I, \pi \right] \leq d_{th}. \tag{15b}$$

The goal of the agent is to find the optimal policy π^* that minimizes the long term cost while satisfying the connectivity constraint.

We propose using the Lyapunov function-based method to derive a robust optimal policy π^*, solution of (15) in domain D_1 at f_1. The rationale behind the Lyapunov approach is to find a set of robust actions that meet the condition (15b) and guarantee global robustness during training. As a consequence, it can be considered a suitable candidate as teacher in the TL process. From here on, for simplicity, we will refer to the robust policy π_1 in domain D_1 as teacher policy π_T. To the best of the authors' knowledge, this is the first time a Lyapunov approach is used to derive a teacher policy for transfer advice for the UAV connectivity-aware path problem.

B. Background of the Lyapunov-Based robust Policy

We introduce the notation of Lyapunov function following the definition in [39]: Given a baseline policy π_B, i.e. $\mathcal{D}_{\pi_B}(q_I) \leq d_{th}$, a function $L : S \to \mathcal{R}$ is said to be a Lyapunov function w.r.t initial state q_I and constraint threshold d_{th} if it satisfies the following conditions:

$$T_{\pi_B, d}[L](q_n) \leq L(q_n) \quad \forall(q_n) \in \mathcal{S}, \tag{16a}$$

$$L(q_I) \leq d_{th}, \tag{16b}$$

$$L(q_F) = 0. \tag{16c}$$

We denote the constraints in (16a) as Lyapunov constraints and (16b) as robustness condition. Term $T_{\pi, d}$ is the generic

Bellman operator w.r.t a policy π and constraint cost function d

$$T_{\pi,d}[V](\mathbf{q}_n) = \sum_a \pi(a \mid \mathbf{q}_n)\big[d(\mathbf{q}_n, a) + \sum_{q'_n \in \mathcal{S}} P(\mathbf{q}'_n \mid \mathbf{q}_n, a)V(\mathbf{q}'_n)\big], \quad (17)$$

where $\mathbf{q}'_n$ is next state $\mathbf{q}_{n+1} \in \mathcal{S}$ under action a.

Given any arbitrary Lyapunov function L, consider the set $F_L(\mathbf{q}_n) = \{\pi(\cdot \mid \mathbf{q}_n) \in \Pi : T_{\pi_B,d}[L](\mathbf{q}_n) \leq L(\mathbf{q}_n)\} \, \forall \mathbf{q}_n \in \mathcal{S}$. Given the contraction property of $T_{\pi_B,d}$ [40], together with $L(\mathbf{q}_I) \leq d_{th}$, any policy π in this set satisfies the robustness conditions and is a feasible solution of (15). This set of robust policies is defined as the L-induced policy set. Since it is not guaranteed that the set $F_L(\mathbf{q}_n)$ contains any optimal solution of (15), the goal of the Lyapunov approach in this paper is to formulate an appropriate function L, such that F_L contains an optimal policy π^* to work as π_T. Finding an appropriate Lyapunov function may not be an easy task. [39][Lemma 1] ensures that without loss of optimality, the Lyapunov function that satisfies the above criterion can be expressed as

$$L_{\pi_B,\epsilon}(\mathbf{q}_n) = \mathbb{E}\big[\sum_{n=0}^N d(\mathbf{q}_n) + \epsilon(\mathbf{q}_n) \mid \pi_B, \mathbf{q}_n\big], \quad (18)$$

in which $\epsilon(\mathbf{q}_n)$ is an auxiliary constraint. Thus, finding L that satisfies the above condition is equivalent to perform appropriate cost-shaping with auxiliary ϵ which can be built using the method proposed in [39]. This method approximates ϵ to a constant function, which is independent of state and can be computed more efficiently as

$$\hat{\epsilon} = \frac{d_{th} - D_{\pi_B}(\mathbf{q}_I)}{\mathbb{E}[T^*|\mathbf{q}_I, \pi_B]}, \mathbf{q}_n \in \mathcal{S}, \quad (19)$$

where $\mathbb{E}[T^* \mid \mathbf{q}_I, \pi_B]$ is the expected stopping time of the CMDP. To speed up the computation of the expected stopping time we replace the denominator of (19) with the upper bound $\overline{N}$, maximum number of allowed steps, leading to $\hat{\epsilon} = \frac{1}{\overline{N}}(d_{th} - D_{\pi_B}(\mathbf{q}_I))$. Substituting this last equation into (18), the Lyapunov function becomes

$$L_{\pi_B,\epsilon}(\mathbf{q}_n) = \mathbb{E}\big[\sum_{n=0}^N d(\mathbf{q}_n) + \hat{\epsilon} \mid \pi_B, \mathbf{q}_n\big], \quad (20)$$

and the set of robust policies $F_L(q_n)$ can be written as

$$F_L(\mathbf{q}_n) = \{\pi(\cdot \mid \mathbf{q}_n) \in \Pi : T_{\pi_B,d}[L_{\hat{\epsilon}}](\mathbf{q}_n) \leq L_{\pi_B,\hat{\epsilon}}(\mathbf{q}_n)\}. \quad (21)$$

The above formulation can be used to propose a robust policy and value iteration algorithm, in which the goal is to solve the Linear Programming (LP) problem [39]

$$\pi^*(\cdot \mid \mathbf{q}_n) \in \arg\min_{\pi \in \Pi} \big\{\pi(\cdot \mid \mathbf{q}_n)^T Q_C(\mathbf{q}_n, \cdot) :$$
$$(\pi(\cdot \mid \mathbf{q}_n) - \pi_B(\cdot \mid \mathbf{q}_n))^T Q_L(\mathbf{q}_n, \cdot) \leq \hat{\epsilon}\big\} \quad (22)$$

where $Q_L(\mathbf{q}_n, a) = d(\mathbf{q}_n) + \hat{\epsilon} + \alpha \sum P(\mathbf{q}'_n \mid \mathbf{q}_n, a) L_{\pi_B, \hat{\epsilon}}$ is the Lyapunov function and $Q_C(\mathbf{q}_n, a) = c(\mathbf{q}_n, a) + \alpha \sum_{\mathbf{q}'_n} P(\mathbf{q}'_n \mid \mathbf{q}_n, a) V_C$ and $V_C(\mathbf{q}_n) = T_{\pi_B,c}[V_C](\mathbf{q}_n)$ are the state action value function and the value function (w.r.t. the cost function c).

Since we assume that the environment in which the UAV is flying is composed by a large and continuous state space, solving (22) becomes numerically intractable. To address this issue, in the next section, we propose a DDQN approach.

C. Lyapunov Approach DDQN for Connectivity-Aware Path Design

In this section we use the above derived Lyapunov function to derive an optimal robust policy via DDQN. Using the notation of action-value function [40], we can write the Lyapunov state-action value function $Q_L(q_n, a)$ as

$$Q_L(\mathbf{q}_n, a) = Q_D(\mathbf{q}_n, a) + \hat{\epsilon} Q_T(\mathbf{q}_n). \quad (23)$$

where $Q_D(\mathbf{q}_n, a)$ represents the constraint state-action value function. The stopping time value network $Q_T(\mathbf{q}_n)$ is a function related to the number of remaining steps and discount factor, and can be computed as $Q_T(\mathbf{q}_n) = \sum_{t=m}^{\overline{N}+1-m} \alpha^{t-m}, \forall \mathbf{q}_n \in S$.

If π_B, $Q_D(\mathbf{q}_n, a)$ and $Q_T(\mathbf{q}_n)$ are known, the auxiliary cost in (19) can be computed as

$$\epsilon'(\mathbf{q}_n) = \epsilon' = \frac{d_{th} - \pi_B(\cdot \mid s_0)^T Q_D(\mathbf{q}_n, a)}{\pi_B(\cdot \mid s_0)^T Q_T(\mathbf{q}_n)}. \quad (24)$$

Finding the optimal policy π^* through (22) and (24) requires accurate calculation of $Q_D(\mathbf{q}_n, a)$, $Q_C(\mathbf{q}_n, a)$ and π_B. One traditional way to derive optimal action-value functions is table-based method, which requires storing and maintaining a state-action value table, one value for each state-action pair. However, for the path design under consideration, the state-action value table would exponentially grow with the size of the flying area. To overcome this issue, parametric functions can be trained to approximate the state-action value. Specifically, we utilize Neural Networks (NNs) to perform function approximation. Let $\hat{Q}_D(\mathbf{q}_n, a; \theta_D)$, $\hat{Q}_C(\mathbf{q}_n, a, \theta_C)$ be the parameterized evaluation networks with weights θ_D and θ_C, then (23) becomes

$$Q_L(\mathbf{q}_n, a, \theta_D) = \hat{Q}_D(\mathbf{q}_n, a, \theta_D) + \hat{\epsilon}' Q_T(\mathbf{q}_n). \quad (25)$$

where $\hat{\epsilon}'$ is computed as

$$\hat{\epsilon}'(\mathbf{q}_n) = \hat{\epsilon}' = \frac{d_{th} - \pi_B(\cdot \mid s_0)^T \hat{Q}_D(\mathbf{q}_n; \theta_D)}{\pi_B(\cdot \mid s_0)^T Q_T(\mathbf{q}_n)}. \quad (26)$$

To train the networks $\hat{Q}_D$, $\hat{Q}_C$ we minimize squared error of prioritized Bellman residuals as for a loss function that can be defined as

$$L_c(\theta_C) = p_{c,n}\big(y_n^c - \hat{Q}_C(\mathbf{q}_n, a, \theta_C)\big)^2, \quad (27)$$

and

$$L_d(\theta_D) = p_{d,n}\big(y_n^d - \hat{Q}_D(\mathbf{q}_n, a, \theta_D)\big)^2, \quad (28)$$

where $p_{c,n}$ and $p_{d,n}$ are the samples priority. In the above equations, term y_n^c is the target cost value, expressed as

$$y_n^c = c_{n:n+N_1} + \alpha^{N_1}\pi(\cdot \mid \mathbf{q}'_n)^T \hat{Q}_C(\mathbf{q}_{n+N_1}, a^*, \theta_C^-), \quad (29)$$

where a^* is

$$a^* = \arg\max \hat{Q}_C(\mathbf{q}_{n+N_1}, a', \theta_C), \quad (30)$$

to separate the action selection and the action evaluation as for double Q-learning technique [41]. Similarly, the target y_n^d for the constraint cost can be denoted as

$$y_n^d = d_{n:n+N_1} + \alpha^{N_1} \pi(\cdot \mid \mathbf{q}_n')^T \hat{Q}_D(\mathbf{q}_{n+N_1}, a^*, \theta_D^-). \quad (31)$$

In each iteration the agent takes action a_n generated by current baseline policy π_B, and perform a DDQN update, computing the loss to update the weights θ_C, θ_D of networks $\hat{Q}_D$, $\hat{Q}_C$. To derive a reasonable baseline policy π_B for the UAV path design under study we create another DNN. As a result, the baseline strategy action probability is approximated by the output of the DNN, namely $\pi_B \approx \hat{\pi}(\cdot \mid \mathbf{q}_n; \theta_\pi)$. We train the policy network by optimizing a loss function that consists on the Kullback-Leibler (KL) divergence between the baseline strategy and the optimal strategy as:

$$L(\theta_\pi) = \mathbb{E}_{\mathbf{q}_n}[D_{KL}(\hat{\pi}(\cdot \mid \mathbf{q}_n; \theta_\pi) \| \pi^*(\cdot \mid \mathbf{q}_n))]. \quad (32)$$

Note that in equations (27)-(31), to improve the stability and convergence of our algorithm, we exploit different techniques. Unlike the conventional Q-learning where target functions are produced by using one-step look-ahead, we use n-step lookaheads, or multi-step learning technique. Specifically, in the target equation (29), (31) the truncated N_1-step cost and constraint cost from a given state $\mathbf{q}_n$ are defined as:

$$c_{n:n+N_1} = \sum_{i=0}^{N_1-1} \alpha^i c_{n+1+i} \quad (33)$$

$$d_{n:n+N_1} = \sum_{i=0}^{N_1-1} \alpha^i d_{n+1+i}. \quad (34)$$

In conventional DRL, after executing the action, the agent stores the state-action-reward transition into a replay memory. In a second step, the agent performs the weight updates selecting a random sample of $|B|$ instances to break the correlation between instances [42]. However, sampling randomly the mini-batch B may affect the convergence of the training procedure. For this reason samples can be selected according to a priority determined by their Temporal Difference (TD) error, which can be computed as $\delta_c = \{y_j^c - \hat{Q}_C(\mathbf{q}_n, a, \theta_C)\}_{j=1}^{|B|}$, $\delta_d = \{y_j^d - \hat{Q}_D(\mathbf{q}_n, a, \theta_D)\}_{j=1}^{|B|}$. In this work, we apply a replay prioritization scheme that considers that target functions are produced by using a multi-step learning technique. Samples and TD errors are stored in a sliding window W for N_1 transitions to enable multi-step learning. The sampling priority $p_{c,n}$ and $p_{d,n}$ in (27), (28) are given by a weighted sum of two different components as

$$\eta \max_i \delta_i + (1-\eta)\bar{\delta} \quad (35)$$

where in the general δ we omitted the subscript c or d to simplifu the notation. δ_c is used for the computation of $p_{c,n}$ and δ_d for $p_{d,n}$. The term $\max_i \delta_i$ is the max absolute N_1-step TD error δ contained within the $|B|$-length sequence, η is a tunable parameter $\in [0,1]$. The second term is the sequence mean absolute N_1-step TD error. Finally, it can be noted in (29), (31) that $\hat{Q}_C(\mathbf{q}_{n+N_1}, a^*, \theta_C^-)$, $\hat{Q}_D(\mathbf{q}_{n+N_1}, a; \theta_D^-)$ are target networks of the evaluation networks. A target network has the
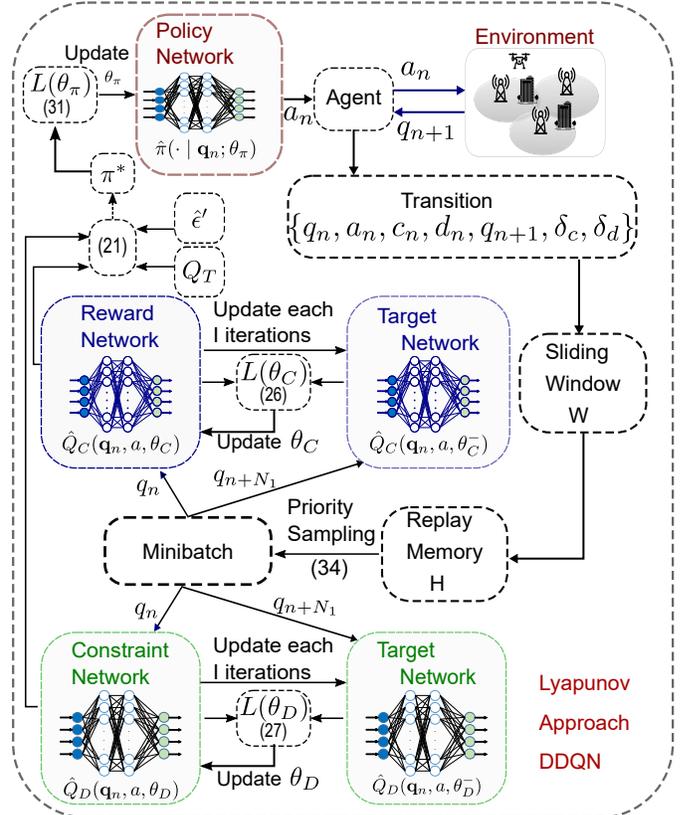

Fig. 2: The Lyapunov robust-DDQN scheme proposed in this paper for connectivity-aware path design with Policy, Cost and Constraint Cost networks.

identical NN structure of the related evaluation network, but its weights θ_C^-, θ_D^- are updated only each I iterations by copying the weights from the evaluation. In this way, the correlation between the target and estimated Q-values is reduced.

The proposed algorithm to derive a robust UAV path via Lyapunov method is summarized in Fig. 2, while Algorithm 1 presents the pseudocode.

IV. TRANSFER LEARNING VIA TEACHER POLICY

In this section we describe the Teacher Advice algorithm to provide external knowledge and allow the agent pre-trained in D_1 to quickly adapt to the new environment D_2.

Let us assume there exists a policy π_T, solution function of (15) mapping states to actions, in a defined domain $D_1 = \langle \mathcal{S}, \mathcal{A}, \mathcal{P}, \mathcal{C}_1, \mathcal{D}_1, \alpha, d_{th} \rangle$ at f_1 to get from a particular starting point to a goal, given a set of outage states. Let us now consider a domain D_2 at frequency f_2 that differs from domain D_1 by the constraint cost distribution: $\mathcal{D}_1, \neq \mathcal{D}_2$. We propose to consider D_1 as the old domain and D_2 as the new domain.

To reduce the computational burden of the training process in the new domain, we propose leveraging Transfer Learning to learn an optimal policy by leveraging exterior information from D_1 as well as internal information from D_2. The robust teacher policy π_T supports the exploration process in domain D_2 at frequency f_2 in two ways (Fig. 3). In the first step, we use robust trajectories generated using a pre-trained π_T to

---

ALGORITHM 1: robust DDQN Algorithm for Connectivity-Aware Path

---

1 **Initialize:** maximum number of episodes, the prioritized replay memory H with capacity N, mini batch size $|B|$;
2 **Initialize:** Upper limit of Radio Failures TH_1, UAV flight speed ;
    for *episode = 1,...,Max episode* **do**
3 | Initialize a sliding window queue W with capacity N_1;
4 | Initialize $q_0 = \{\mathbf{q}_I\} \in \mathcal{S} \setminus \mathcal{S}_\mathcal{O}$, set step $k \leftarrow 0$;
5 | **for** *each step of episode* **do**
6 | | Select action a_n according to parameterized network $\hat{\pi}(\cdot \mid q_n; \theta_\pi)$;
7 | | Agent execute action a_n, observe $\{\mathbf{q_{n+1}}\}$ and c_n, d_n;
8 | | Store experience $(\mathbf{q}_n, a_n, c_n, d_n, \mathbf{q}_{n+1}, \delta_c, \delta_d)$ in sliding window queue W;
9 | | When reached a number N_1 of transitions, store them in replay memory H and compute (33) and (34);
10 | | From buffer H sample minibatch B of N_1 experience according to the priority as for (35);
11 | | Update the DNN of state action cost function Q_C performing gradient descent on loss (27) with respect to θ_C;
12 | | Update the DNN of state action constraint function Q_D performing gradient descent on loss (28) with respect to θ_D;
13 | | Update the priority weights $p_{c,n}$, $p_{d,n}$ based on TD error;
14 | | Obtain π^* by (22);
15 | | Update $\hat{\pi}(\cdot \mid q_n; \theta_\pi)$ via $\theta_\pi \leftarrow \theta_\pi - \alpha \nabla_{\theta_\pi} L(\theta_\pi)$;
16 | **end**
17 | Update the target networks after I iterations.
18 | Set $\pi_T = \pi^*$ and $\theta_T = \theta_\pi$;
19 **end**

Fig. 3: Illustration of our proposed Transfer Learning Algorithm: a pre-trained policy in domain D_1 is used as teacher in domain D_2.

provide prior knowledge about the task. To reach this goal, we utilize the concepts of known and unknown spaces [43] to cover some regions of the feature space. In a second step, the agent transfers the pre-trained weights from D_1 and starts its training in the new domain D_2. The teacher policy π_T is used to support the exploration process when the agent meets an unknown state. In new situations, the learning agent evaluates a state from the perspective of the old domain to reduce the frequency of risky states. Here it is important to note that the role of the teacher policy is not to supply the best action but to advice an action more robust than the one obtained through random exploration. Fig. 3 summarizes the overall TL process adopted in this paper. Note that the proposed TL method is

applicable to any DRL algorithm and it is not specific to the robust-DDQN only.

A. Initial Known Space

The agent, equipped with an empty memory C of size Z, builds the initially known space by storing new experiences. Using π_T, we run $Q < Z$ iterations with the environment and collect states, actions taken, reward received (cost and constraint cost in this case), and if the current state is terminal. The stored data follows the structure of the experience replay memory used in conventional DQN. Each memory element represents a transition the agent has experienced in domain D_1. The resulting data forms the known space. When the agent enters a new state $\mathbf{q}_n$, it computes the euclidean distance to determine if $\mathbf{q}_n$ belongs to the known space. Hence, we define a density threshold Θ and a risk function as [43]

$$\Lambda^{\pi_T}(a_n | \mathbf{q_q}) = \begin{cases} 0, & \text{if } \min_{1 \le q \le Z} d_{n,q} \le \Theta \\ 1, & \text{otherwise.} \end{cases} \quad (36)$$

where $d_{n,q} = \|\mathbf{q_n} - \mathbf{q_q}\|$ is the Euclidean distance between a new state and the states in memory. The parameter Θ defines the classification region for a new state $\mathbf{q}_n$ and it is dependent on the size of the action. In this work, we consider $\Theta = 2\Delta_T V_{\max}$. When the distance of the nearest neighbor to $\mathbf{q}_n$ is greater than Θ, the experience is added to the memory.

Thus, the definition of a known state is as following:

Definition 4.1: Given a density threshold Θ, a state $\mathbf{q}_n$ is considered known when $\Lambda^{\pi_T}(\mathbf{q}_n) = 0$ and unknown in all other cases. Formally, $\Sigma \subseteq \mathcal{S}$ is the set of known states, while $\Upsilon \subseteq \mathcal{S}$ is the set of unknown states with $\Sigma \cap \Upsilon = 0$.

Using the known space set, we could transfer the learner the advice to prefer some actions over others in specific regions of the feature space. However, a direct translation of the action in the new domain would heavily limit the agent ability in domain D_2. To make our approach robust to imperfections in the advice or teacher policy, we are interested in providing the learning agent with the possibility to refine the transferred knowledge based on its subsequent trajectories in domain D_2. In what follows, we present the algorithm for the training of the learner agent in domain D_2.
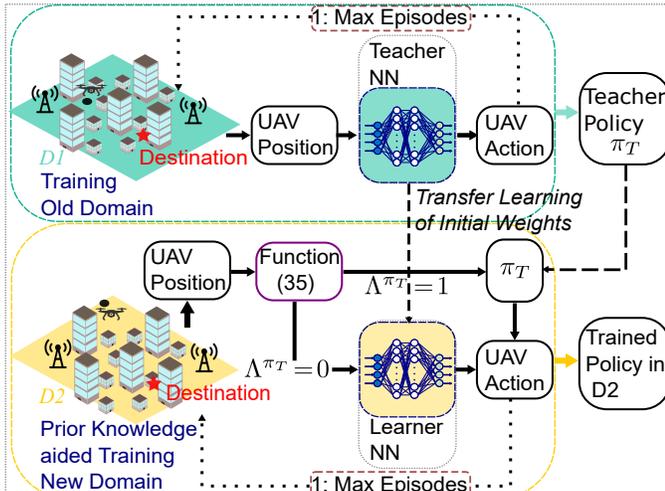
B. Training in New Domain

The algorithm to train the learning agent in the new domain is composed of an initialization step and a reinforcement learning step. The different steps that can be summarized as follows:

a. **Initialization Step**: In this step the hyperparameters, the density threshold Θ and the initial state $\mathbf{q}_I$ are initialized. The algorithm transfers the weights of the teacher DNN pre-trained in D_1 to domain D_2, in DNN networks with identical structure. In addition, to obtain new and improved ways to complete the task, we add Gaussian noise to the initial weights such that $\theta_{\pi_{f_2}} = \theta_{\pi_T} + \mathcal{N}(0, \sigma^2)$.

b. **Reinforcement Learning Step**: In this step, the training in D_2 starts and the algorithm refines the policy to satisfy the connectivity constraint in domain D_2. When the UAV

ALGORITHM 2: Transfer Learning for Connectivity-Aware Path Design

---

1 Given baseline behavior π_T and memory C with maximum size Z;
2 **Initialize** maximum number of episodes, density threshold Θ, prioritized replay memory H with capacity N, mini batch size $|B|$;
3 Create Σ collecting Q interactions;
4 Transfer Initial weights from π_T;
5 **Set** maxTotalRwEpisode = 0;
6 **for** *episode = 1,...,Max episode* **do**
7   Initialize $q_0 = \{\mathbf{q}_I\} \notin \mathcal{S}_\mathcal{O}$, set step $k \leftarrow 0$;
8   **for** *each step of episode* **do**
9   Compute the closest $\mathbf{q}_q \in C$ to $\mathbf{q}_n$ using (36);
10   **if** *($\mathbf{q}_n$ is known)* **then**
11   Select action using $\pi = \hat{\pi}(\cdot \mid q_n; \theta_{\pi_{f_2}})$;
12   Execute lines 8-15 of Algorithm 1;
13   **else**
14   Choose an action using π_T;
15   Agent execute action a_n, observe $\{\mathbf{q_{n+1}}\}$ and c_n,d_n;
16   Add experience to memory C;
17   **end**
18   **end**
19   Remove least frequently used experiences in C;
20 **end**
21   Update the target networks after I iterations.
22   Set $\pi_2 = \pi^*$;
23 **end**

---

flies in a new position, if the state is known, $\mathbf{q}_n \in \Sigma$, the agent performs an action a_n using policy network $\hat{\pi}(\cdot \mid q_n; \theta_{\pi_{f_2}})$ and train the networks in domain D_2. In unknown states, instead, the action a_n is performed using the teacher policy π_T and the experience is added to the known set in memory Z. As the exploration process and the training in D_2 continue, the knowledge of the agent of D_2 and the accuracy of π_2 improve. Hence, the algorithm utilizes the teacher policy π_T only as a backup policy with to guide the learning away from risky states or, at least, reduce their frequency.

The pseudo code for the Transfer Learning and Teacher advice is reported in Algorithm 2.

V. NUMERICAL RESULTS

In this section we present the main numerical results of our findings. We first describe the radio environment used for generating the UAV trajectories. Then, we evaluate the performance of the proposed robust-DDQN algorithm in domain D_1 at f_1. We compare our approach with state of the art deep RL. Specifically, we implement an unconstrained Dueling DDQN that has been shown to suit UAV connectivity-aware path problems [18], [35]. We model the reward function to minimize the flight time and the number of radio failures for a fair comparison. Details about the implementation of the Dueling DDQN benchmark strategy will be presented in Appendix B. At last, we validate and show the benefit of the transfer learning approach from D_1 at f_1 to D_2 at f_2.

A. Radio Environment

The radio environment where the UAV is flying is composed of buildings generated based on the International Telecommunication Union (ITU) model [44], which involves three

TABLE III: Parameters utilized in the simulation environment

Radio Simulation Parameters		
Parameter	Description	Value
L	Area Size	1 [km]
$V_{\max}$	UAV Speed	20 [m/s]
h_n	UAV Height	100 [m]
ϕ_1 / ϕ_2	Antenna Tilt f_1 / f_2	-10/10°
G_{max}	max directional gain antenna element	8 dBi
σ^2	Noise Power sub-6/mmWave	-204/-120 [db/Hz]
m_v	Nakagami Fading param.	3
Δ_T	Time Step Length	0.5 [s]
$\bar{\gamma}$	SINR Threshold	0 dB
$\bar{P}_{th}$	Ouatge Threshold	0.9
d_{th}	Connectivity Outage Threshold	10%

parameters: i)the ratio of land area covered by buildings to total land area, ii) the mean number of buildings per unit area, iii) the height of buildings modeled by a Rayleigh Probability Density Function (PDF). The above parameters can be modified as specified in [45] to create Suburban, Urban, Dense Urban and High Rise Urban environments. We have considered the last three mentioned environments as they are the most challenging for connectivity-aware UAV path and to demonstrate the generality of our approach. Each environment has a different BS number, BS power and height within a geographical area of $L \times L$, as for BS density specified in [46]. At frequency $f_1 = 2$ GHz, we consider 8 antenna elements at the ground BS, while 64 antennas at $f_2 = 28$ GHz [37], as for the ULA and UPA antenna models described in Section II-A1. At sub-6 GHz, we adopt the 3GPP Macro Path Loss Model for Urban scenario [47], that includes modeling for LoS and NLoS channels. The presence/absence of obstacles is determined in the simulated environment by checking whether the line BS-UAV is blocked or not by any building. A ray tracing software would allow us to include in the propagation calculation the relative permittivity and conductivity of the surface material, which is different for any building. However, this information would limit the algorithm's training to a specific scenario or condition. The statistical ITU building model [44] used in our approach reflects the average characteristics over a large number of geographic areas of similar type and has been widely used to characterize urban environments in UAV trajectory path design [18], [16]. Using data extracted by a simulator allows us to train the proposed robust-DDQN and transfer learning method on a broader general scenario, improving the algorithm's generalisation. At mmWave we consider the path loss model in (2) with $\alpha_L = 2$, $\alpha_{NL} = 4$, X_L, $X_{NL} = 5e^{-4}$. We have adopted a bandwidth of 10 MHz at sub-6 GHz, 100 MHz at mmWave and a transmit power of 36 dBm at sub-6 GHz and 30 dBm at mmWave, which are in line with the specifications envisioned for downlink transmission in Fifth Generation (5G) mmWave mobile networks. We consider a UAV speed of 20 m/s [19] and ease of illustration but without loss of generality, a fixed fly altitude.

The remaining simulation parameters can be found in Table III.

B. Performance of the robust Teacher Policy

In this section, we show the performance of the robust Teacher Policy derived using a robust-DDQN approach. Ta-

TABLE IV: Hyperparameters utilized in the simulation environment

Hyperparameters robust-DDQN		
Parameter	Description	Value
N_1	n-STEP	10
$\overline{N}$	Max Steps	100
α	Discount Factor	0.99
$|B|$	Minibatch Size	32
H	Replay Memory Size	200000
c	Move Penalty	0.5
d	Radio Failure Penalty	1
η	Priority Sample Weight	0.9 [42]

ble IV shows some hyperparameters used to generate the results. More details about the implementation of the robust-DDQN approach can be found in Appendix A. The mission is considered successful if the UAV reaches the destination before the constraint threshold is exhausted. The destination is placed in $\mathbf{q}_F = [700, 800, 100]$ m and the actions at each step are left-right-forward-back. To make the path task more challenging, we consider in Fig. 4 a conservative constraint threshold $d_{th} = 10$. Note that the training phase of the robust-DDQN model is executed for a number of 5000 episodes, each of which accounts for a maximum of $N = 100$ steps. The fairness of the experiment episodes is ensured by running the trials with a different preset random seed. The mission success rate is averaged over 500 evaluation episodes with a random initial starting point. The initial starting point is chosen from a continuous space in the area $L \times L$. Note that, to ease the algorithm generalization, the initial position is not fixed but is chosen randomly in the flying area for each evaluation episode. We also mention that the final position is chosen inside a fixed area of side $\pm\Delta = 30$ m. Fig. 4 shows the normalized success rate for the proposed robust-DDQN compared with a conventional unconstrained Dueling DDQN. The x-axis shows the number of episodes, while the y-axis shows the mission success. While both algorithms converge with good performance, the proposed robust-DDQN algorithm has a generally higher success rate. In addition Fig. 5a shows that our Lyapunov-based algorithm can control the radio failures even when the environment is more challenging. On the contrary, the unconstrained benchmark DDQN is more apt to violate the constraint during training.

Fig. 5b shows the reward received by the agent for different urban environments. The robust-DDQN can adequately learn the path design task with good return while satisfying the connectivity requirement. The shaded areas in Fig. 5b represent the 1-SD confidence intervals over 500 runs. Finally, Fig. 6 evaluates how the method generalizes to different values of connectivity outage threshold d_{th}. Conservative thresholds lead to longer trajectories, while higher d_{th} allow more flexibility and shorter trajectories.

C. Performance of Transfer Learning

In this subsection we investigate the potential of the transfer learning algorithm in domain D_2. Details about the implementation of the Teacher advice and Transfer Learning algorithm are in Appendix C. The impact of the transfer learning is measured considering the asymptotic performance of the agent at mmWave. The TL algorithm is executed for 5000 trials
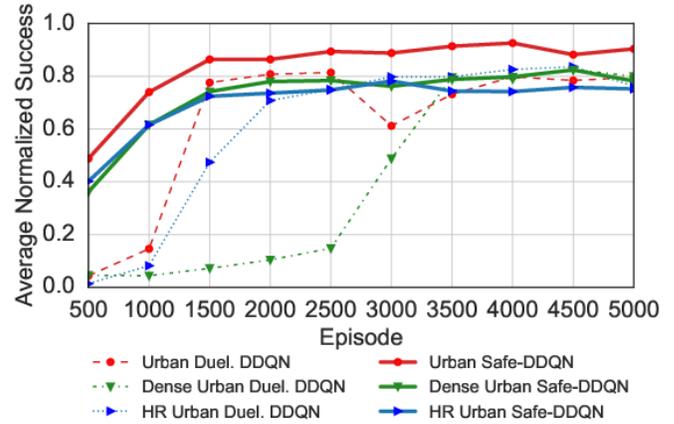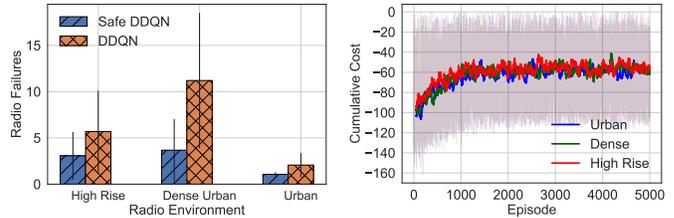

Fig. 4: Results of the robust-DDQN compared with Dueling DDQN for three urban environment with different building distribution. Term HR stands for High Rise

(a) UAV navigation constraint cost satisfaction comparison

(b) Average cumulative reward for three different urban environments

Fig. 5: Convergence of the proposed robust DDQN algorithm: (a) maximum radio failure satisfaction and (b) reward control

and is compared with the algorithm executed without TL. The mission rate is again averaged over 500 episodes with the same constraint threshold as the previous section. We investigate first the case of using a teacher policy pre-trained in sub-6 GHz via robust-DDQN. The results are shown in Fig. 7. The curves show the average mission success of over 500 episodes. The transfer learning is here very effective since the algorithm with TL needs few training trials to reach the asymptotic performance of the algorithm trained tabula rasa.

In addition, Fig. 8 shows the results of the teacher advice transfer approach using a Dueling DDQN as a teacher. Transfer Learning is again very powerful, as the Dueling DDQN without transfer needs at least 300 episodes to perform comparably to the algorithm with transfer.

Fig. 9 shows an example of the radio map for the High Rise environment. Fig. 9 is coloured according to the average SINR. Lighter colour means a higher SINR and vice versa. Generally, it is visible a different behaviour between the two bands. At Sub-6GHz, lower SINR is in interference regions between the BSs. At mmWave, the lower SINR areas are more irregular due to the combined effects of the higher BS antenna tilt and building blockage. In Fig. 9a we plot the radio map at sub-6 GHz for a UAV height of 100 m together with two paths that start from two different initial points. The UAV reaches the destination from two different starting points during the training in the old domain. Recalling that a radio failure occurs at average SINR values below the SINR threshold 0 dB, it is
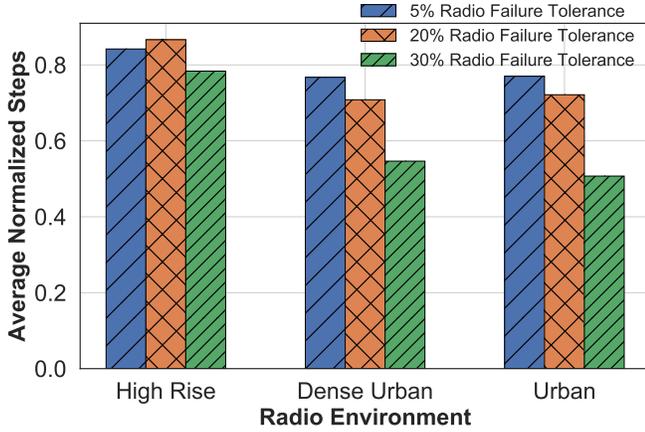
Fig. 6: Impact of the Connectivity Outage Threshold on the proposed robust DDQN path Design
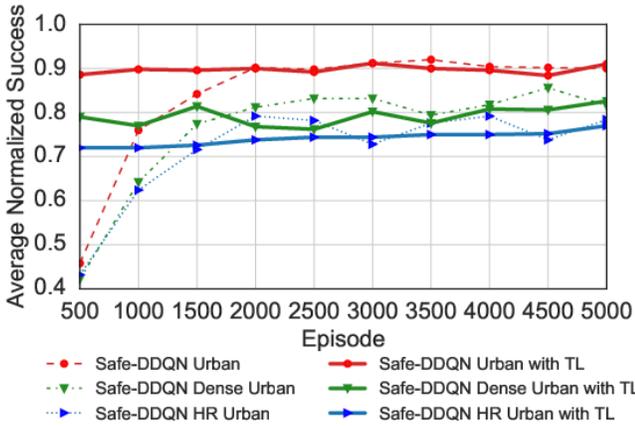

Fig. 7: robust-DDQN: Average Asymptotic Performance of the Transfer Learning algorithm measured in % of accomplished missions for different urban environments at mmWave.
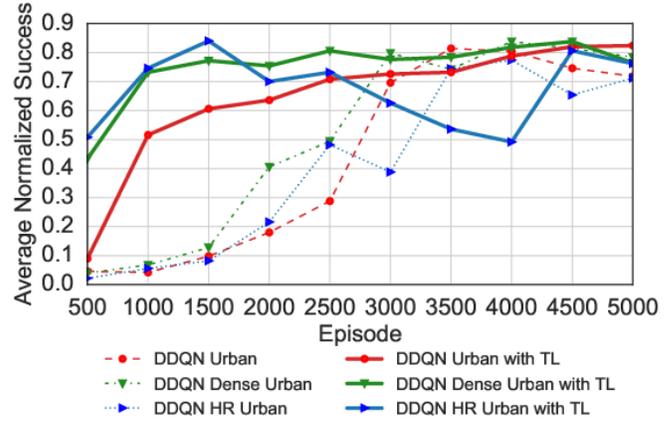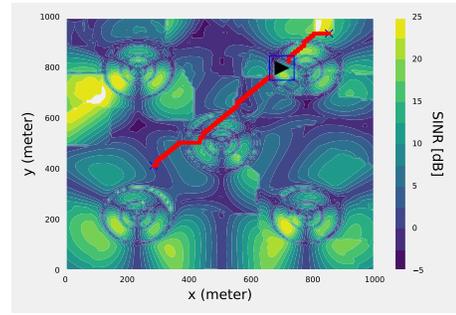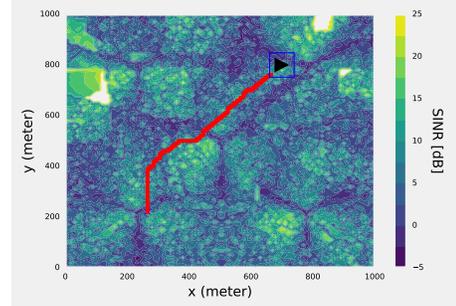

Fig. 8: Dueling DDQN: Average Asymptotic Performance of the Transfer Learning algorithm measured in % of accomplished missions for different urban environments at mmWave

(a) UAV path design example at sub-6 GHz along with the radio map. The UAV reaches the destination from two different starting points during the training in the old domain.

(b) Returned UAV path design in the new domain at mmWave along with the radio map.

Fig. 9: An illustrative example of the radio maps in a High Rise environment for the sub-6 GHz and mmWave and the returned UAV path. Radio failures occur below the SINR threshold of 0 dB.

possible to see that the UAV adjusts its trajectory to satisfy the connectivity constraint. In Fig. 9b we plot the radio at mmWave band for the same UAV height and the returned path. The UAV is reusing some of the previous knowledge to reach the destination.

In conclusion, results show that the transfer advice framework proposed in this paper helps a learner agent reduce the training time in successful missions using both the proposed robust-DDQN and a conventional Dueling DDQN as a teacher. Different environments with different levels of complexity in terms of coverage aware UAV navigation have been tested. This shows that the proposed TL framework is versatile and not dependent on the algorithm used to train the teacher policy. However, it is important to observe that the robust-DDQN, creating a policy that respects the connectivity constraint throughout training, results in a better teacher policy.

VI. CONCLUSION

In this paper, we have developed a DDQN Lyapunov based approach to solve the non-convex UAV connectivity-aware path design across different simulation environments. We then proposed a Transfer Learning technique to improve the agent learning in a new domain at mmWave using the knowledge gained in a domain D_1 at sub-6 GHz. We have evaluated the efficiency of our TL approach using a Lyapunov based DDQN teacher policies derived at sub-6 GHz benchmarked with a Dueling DDQN. Our approach showed the potential of the proposed TL framework to save many training episodes for both the teacher policies, resulting in fewer UAV flights. The learning agent's convergence using a teacher policy derived via the Lyapunov based DDQN is faster for all the different

TABLE V: Networks Structure in robust-DDQN Algorithm

Type	Output Size	Activation	Learning Rate
Reward	$\dim(\mathcal{A})$	Linear	10^{-4}
Cost	$\dim(\mathcal{A})$	Linear	10^{-4}
Policy	$\dim(\mathcal{A})$	Softmax	10^{-6}

urban scenarios under consideration. Future works include the evaluation of the sensitivity of our algorithm to the advice of a non-perfectly trained teacher.

ACKNOWLEDGEMENT

APPENDIX A
ROBUST DDQN IMPLEMENTATION

Table V displays the architecture of the neural networks used in our robust-DDQN algorithm. Especially, Table V shows the learning rate values adjusted in the algorithm to reach convergence. The hyperparameters in Table IV are selected to both achieve a good trade off between learning performance and model complexity. We implement the proposed robust-DDQN based on Tensorflow library in Python. The Cost and Constraint Cost layers are all fully connected and consist of four hidden layers with ReLU as an activation function. The layers have respectively 64, 64, 32 and 4 nodes, respectively. The policy network consists of eight hidden layers, activated with ReLu and with respectively 512, 256, 128, 128, 64, 64, 32 nodes. Weights of the policy network are initialized using the inverse distance from the UAV location to the destination, that is considered known, so that $\hat{\pi}(\cdot \mid q_n; \theta_\pi)$ approximates $\frac{1}{\|q' - \mathbf{q}_F\|}$, where q' is the next state after taking action a_n. The policy networks weights are updated each 5 episodes, while the Cost and Constraint Cost's ones each 25 episodes. Adam optimizer [48] is used to apply gradient descent for all the networks. The learning rate is reported in Table V.

APPENDIX B
DDQN IMPLEMENTATION

The DNN of the DDQN used for benchmark consists in a Dueling architecture with input layer, four hidden layers, one output layer, all fully connected feedforward, activated using Rectified Linear Units (ReLU) and trained with Adam optimizer to minimize the MSE. The learning rate is kept 0.01. The number of neurons of the hidden layers are 512, 256, 128 and 128. The dueling architecture represents two separate estimators, one neuron for the state value function and K for the action advantages for the K actions. The output of the K+1 neurons represents the aggregated output layer to estimate the K action values. The replay memory and memory C for the transfer learning have size 100,000. At mmWave we encourage exploration through Gaussian noise $\mathcal{N}(0, 0.1)$ to the weights of the network.

APPENDIX C
TEACHER ADVICE AND TRANSFER LEARNING ALGORITHM IMPLEMENTATION

The set of known cases Σ is created running a number $N = 250$ trajectories using the teacher policy π_T and collecting $Q = 9000$ iterations with the environment. The teacher policy might be derived either via the Lyapunov approach or the conventional DDQN described in the previous sections. The memory C has size 200,000. Thus, in a second phase, the network models trained in D_1 are translated into domain D_2. Here, the weights of the networks are perturbed with Gaussian noise, $\mathcal{N}(0, 0.1)$. The training is computed using a prioritized memory of same size as for V.

REFERENCES

[1] Y. Zeng, R. Zhang, and T. J. Lim, "Wireless Communications with Unmanned Aerial Vehicles: Opportunities and Challenges," *IEEE Commun. Mag.*, vol. 54, no. 5, pp. 36–42, May 2016.

[2] Y. Zeng, J. Lyu, and R. Zhang, "Cellular-Connected UAV: Potential, Challenges, and Promising Technologies," *IEEE Wireless Commun.*, vol. 26, no. 1, pp. 120–127, 2018.

[3] Z. Rahimi, M. J. Sobouti, R. Ghanbari *et al.*, "An Efficient 3D Positioning Approach to Minimize Required UAVs for IoT Network Coverage," *IEEE Internet Things J.*, vol. 9, no. 1, pp. 558–571, 2021.

[4] G. Fontanesi, H. Ahmadi, and A. Zhu, "Over the Sea UAV Based Communication," in *EuCNC Proc.* IEEE, 2019, pp. 374–378.

[5] G. Fontanesi, A. Zhu, and H. Ahmadi, "Outage Analysis for Millimeter-Wave Fronthaul Link of UAV-Aided Wireless Networks," *IEEE Access*, vol. 8, pp. 111 693–111 706, June 2020.

[6] G. Geraci, A. Garcia-Rodriguez, L. G. Giordano *et al.*, "Understanding UAV Cellular Communications: From Existing Networks to Massive MIMO," *IEEE Access*, vol. 6, pp. 67 853–67 865, 2018.

[7] S. Zhang, Y. Zeng, and R. Zhang, "Cellular-enabled UAV Communication: A Connectivity-Constrained Trajectory Optimization Perspective," *IEEE Trans. Commun.*, vol. 67, no. 3, pp. 2580–2604, 2018.

[8] M. M. U. Chowdhury, S. J. Maeng, E. Bulut *et al.*, "3-D Trajectory Optimization in UAV-assisted Cellular Networks Considering Antenna Radiation Pattern and Backhaul Constraint," *IEEE Trans. Aerosp. Electron. Systems*, vol. 56, no. 5, pp. 3735–3750, 2020.

[9] S. Zhang and R. Zhang, "Trajectory Design for Cellular-Connected UAV under Outage Duration Constraint," in *Proc. IEEE Int. Conf. Commun (ICC)*, May 2019.

[10] A. Mardani, M. Chiaberge, and P. Giaccone, "Communication-aware UAV Path Planning," *IEEE Access*, vol. 7, pp. 52 609–52 621, 2019.

[11] E. Bulut and I. Guevenc, "Trajectory Optimization for Cellular-Connected UAVs with Disconnectivity Constraint," in *Proc. IEEE Int. Conf. Commun (ICC)*, May 2018.

[12] S. Zhang and R. Zhang, "Radio Map Based Path Planning for Cellular-Connected UAV," in *Proc. IEEE Global Telecommun. Conf. (GLOBECOM)*, Dec. 2019.

[13] O. Esrafilian, R. Gangula, and D. Gesbert, "Learning to Communicate in UAV-aided Wireless Networks: Map-based Approaches," *IEEE Internet Things J.*, vol. 6, no. 2, pp. 1791–1802, Apr. 2019.

[14] H. Yang, J. Zhang, S. Song *et al.*, "Connectivity-Aware UAV Path Planning with Aerial Coverage Maps," in *Proc. IEEE WCNC*, Apr. 2019, pp. 1–6.

[15] S. De Bast, E. Vinogradov, and S. Pollin, "Cellular Coverage-Aware Path Planning for UAVs," in *IEEE SPAWC Workshop*, 2019, pp. 1–5.

[16] O. Esrafilian, R. Gangula, and D. Gesbert, "3D-Map Assisted UAV Trajectory Design Under Cellular Connectivity Constraints," in *Proc. IEEE Int. Conf. Commun (ICC)*, Jun. 2020.

[17] B. Khamidehi and E. S. Sousa, "A Double Q-Learning Approach for Navigation of Aerial Vehicles with Connectivity Constraint," in *Proc. IEEE Int. Conf. Commun (ICC)*, Jun. 2020.

[18] Y. Zeng, X. Xu, S. Jin *et al.*, "Simultaneous Navigation and Radio Mapping for Cellular-Connected UAV with Deep Reinforcement Learning," *IEEE Trans. Wireless Commun.*, 2021.

[19] Y.-J. Chen and D.-Y. Huang, "Joint Trajectory Design and BS Association for Cellular-Connected UAV: An Imitation Augmented Deep Reinforcement Learning Approach," *IEEE Internet Things J.*, 2021.

[20] B. Khamidehi and E. S. Sousa, "Federated Learning for Cellular-Connected UAVs: Radio Mapping and Path Planning," in *Proc. IEEE Global Telecommun. Conf. (GLOBECOM)*, Dec. 2020.

[21] O. Semiari, W. Saad, M. Bennis *et al.*, "Integrated Millimeter Wave and Sub-6 GHz wireless Networks: A Roadmap for Joint Mobile Broadband and Ultra-Reliable Low-Latency Communications," *IEEE Wireless Commun.*, vol. 26, no. 2, pp. 109–115, 2019.

[22] M. Alrabeiah and A. Alkhateeb, "Deep Learning for mmwave Beam and Blockage Prediction Using Sub-6 GHz Channels," *IEEE Trans. Commun.*, vol. 68, no. 9, pp. 5504–5518, 2020.

[23] Z. Zhu, K. Lin, and J. Zhou, "Transfer Learning in Deep Reinforcement Learning: A Survey," *arXiv preprint arXiv:2009.07888*, 2020.

[24] X. Zhang, G. Zheng, and S. Lambotharan, "Trajectory Design for UAV-Assisted Emergency Communications: A Transfer Learning Approach," in *Proc. IEEE Global Telecommun. Conf. (GLOBECOM)*, Dec. 2020.

[25] A. M. Azab, H. Ahmadi, L. Mihaylova *et al.*, "Dynamic Time Warping-based Transfer Learning for Improving Common Spatial Patterns in Brain-Computer Interface," *J. Neural Eng.*, vol. 17, no. 1, p. 016061, 2020.

[26] J. Qiu, J. Lyu, and L. Fu, "Placement Optimization of Aerial Base Stations with Deep Reinforcement Learning," in *Proc. IEEE Int. Conf. Commun (ICC)*, June 2020.

[27] Y. Zeng and X. Xu, "Path Design for Cellular-Connected UAV with Reinforcement Learning," in *Proc. IEEE Global Telecommun. Conf. (GLOBECOM)*, Dec. 2019.

[28] Y.-J. Chen and D.-Y. Huang, "Trajectory Optimization for Cellular-enabled UAV with Connectivity Outage Constraint," *IEEE Access*, vol. 8, pp. 29 205–29 218, 2020.

[29] A. Chapnevis, İ. Güvenç, L. Njilla *et al.*, "Collaborative Trajectory Optimization for Outage-aware Cellular-Enabled UAVs," in *Proc. IEEE Veh. Technol. Conf. (VTC-Spring)*, Apr. 2021.

[30] X. Wang and M. C. Gursoy, "Learning-Based UAV Trajectory Optimization with Collision Avoidance and Connectivity Constraints," *to be published, arXiv:2104.06256*, Apr. 2021.

[31] Y. Gao, L. Xiao, F. Wu *et al.*, "Cellular-Connected UAV Trajectory Design with Connectivity Constraint: A Deep Reinforcement Learning Approach," *IEEE Trans. Green Commun. Netw.*, 2021.

[32] X. Liu, Y. Liu, and Y. Chen, "Reinforcement Learning in Multiple-UAV networks: Deployment and Movement Design," *IEEE Trans. Veh. Technol.*, vol. 68, no. 8, pp. 8036–8049, 2019.

[33] B. Khamidehi and E. S. Sousa, "Trajectory Design for the Aerial Base Stations to Improve Cellular Network Performance," *IEEE Trans. Veh. Technol.*, vol. 70, no. 1, pp. 945–956, 2021.

[34] N. Cherif, W. Jaafar, H. Yanikomeroglu *et al.*, "Disconnectivity-Aware Energy-Efficient Cargo-UAV Trajectory Planning with Minimum Hand-offs," in *Proc. IEEE Int. Conf. Commun (ICC)*, Dec. 2021.

[35] G. Fontanesi, A. Zhu, and H. Ahmadi, "Deep Reinforcement Learning for Dynamic Band Switch in Cellular-Connected UAV," in *Proc. IEEE Veh. Technol. Conf. (VTC-Fall)*, Sept. 2021.

[36] "Study on 3D Channel Model for LTE (release 12)," 3GPP, TR 36.873, Dec. 2017.

[37] M. Rebato, L. Resteghini, C. Mazzucco *et al.*, "Study of Realistic Antenna Patterns in 5G mmwave Cellular Scenarios," in *Proc. IEEE Int. Conf. Commun (ICC)*, May 2018.

[38] T. Zhang, J. Lei, Y. Liu *et al.*, "Trajectory Optimization for UAV Emergency Communication with Limited User Equipment Energy: A safe-DQN Approach," *IEEE Trans. Green Commun. and Network.*, 2021.

[39] Y. Chow, O. Nachum, E. Duenez-Guzman *et al.*, "A Lyapunov-based Approach to Safe Reinforcement Learning," in *Proc. International Conf. on Neural Information Processing Systems*, Dec. 2018.

[40] R. S. Sutton and A. G. Barto, *Reinforcement Learning: An Introduction*. MIT press, 2018.

[41] H. Hasselt, "Double Q-learning," in *Proc. Adv. Neural Inf. Process. Syst. (NIPS)*, Dec. 2010.

[42] S. Kapturowski, G. Ostrovski, J. Quan *et al.*, "Recurrent Experience Replay in Distributed Reinforcement Learning," in *International Conf. on learning representations*, 2018.

[43] J. Garcia and F. Fernández, "Safe Exploration of State and Action Spaces in Reinforcement Learning," *J. Artif. Intell. Res.*, vol. 45, pp. 515–564, 2012.

[44] *Propagation Data and Prediction Methods Required for the Design of Terrestrial Broadband Radio Access Systems Operating in a Frequency Range From 3 to 60 GHz*, ITU-R Recommendation P.1410-5, 2012.

[45] J. Holis and P. Pechac, "Elevation Dependent Shadowing Model for Mobile Communications via High Altitude Platforms in Built-Up Areas," *IEEE Trans. Antennas Propagat.*, vol. 56, no. 4, pp. 1078–1084, 2008.

[46] "Evolved universal terrestrial radio access (E-UTRA); further advancements for E-UTRA physical layer aspects (release 15)," 3GPP, TR 36.814, Mar 2017.

[47] "Technical Specification Group Radio Access Network; Study on Enhanced LTE support for Aerial Vehicles (Release 15)," 3GPP, TR 36.777, Jan. 2018.

[48] D. P. Kingma and J. Ba, "Adam: A Method for Stochastic Optimization," in *Proc. International Conf. on Learning Representations (ICLR)*, 2015.